Human Vitreous: MR Imaging of Oxygen Partial Pressure[1]

Eric R. Muir, PhD
Yi Zhang, PhD
Oscar San Emeterio Nateras, BS
Qi Peng, PhD
Timothy Q. Duong, PhD

Purpose: To develop a magnetic resonance (MR) imaging approach to noninvasively image quantitative Po_2 in the human vitreous.

Materials and Methods: Human studies were approved by the institutional review board with informed consent obtained from all subjects and were HIPAA compliant. Animal studies were performed with animal care committee approval. An MR imaging method to measure the longitudinal relaxation rate, or R1, of water was implemented with a 3.0-T MR imager. R1 was calibrated in water phantoms at multiple Po_2 and temperature conditions (n = 10) and in ex vivo animal vitreous (n = 2). Vitreous Po_2 was imaged in three human volunteers (age range, 26–28 years) in multiple sessions on separate days to evaluate reproducibility. The effects of temperature and ambient air were evaluated by acquiring data with the eye open and closed. Statistical analysis consisted of t tests, with P less than .05 indicating significant difference.

Results: Calibrations of phantoms and ex vivo vitreous yielded an R1 association with oxygen of 0.209 sec^{-1} + Po_2 · 2.07 × 10^{-4} sec^{-1}/mm Hg at 37°C, and an association with temperature (Δ[1/R1]/ΔTemperature) of 0.106 sec/°C ± 0.009 (standard deviation). A difference in R1 was found between the phantoms and vitreous. If uncorrected, vitreal Po_2 would be significantly overestimated ($P < .001$). In vivo human vitreous Po_2 maps were spatially heterogeneous, with a whole vitreous Po_2 of 16.7 mm Hg ± 6.5 (eye closed). Measurements between open and closed eyes showed spatially dependent R1 differences, which translated to temperature differences of 0.34°–0.83°C across the eye.

Conclusion: This study established an MR imaging protocol to image quantitative vitreous Po_2 noninvasively and evaluated effects from vitreal macromolecules, temperature gradients, and ambient air on vitreal Po_2 values. Measurement of vitreous Po_2 with MR imaging has the potential to be used to study eye diseases noninvasively.

[1] From the Research Imaging Institute (E.R.M., Y.Z., O.S.E.N., T.Q.D.) and Departments of Ophthalmology (T.Q.D.), Radiology (Y.Z., O.S.E.N., T.Q.D.), and Physiology (T.Q.D.), University of Texas Health Science Center, 8403 Floyd Curl Dr, San Antonio, TX 78229; South Texas Veterans Health Care System, San Antonio, Tex (T.Q.D.); Southwest National Primate Research Center, San Antonio, Tex (T.Q.D.); and Department of Radiology, Albert Einstein College of Medicine and Montefiore Medical Center, New York, NY (Q.P.). Supported in part by MERIT Award from the Department of Veterans Affairs and Pilot Grant via the Clinical Translational Science Award. E.R.M. was supported in part by the NIH. Received April 4, 2012; revision requested June 5; revision received July 16; accepted July 26; final version accepted August 22. **Address correspondence to** T.Q.D. (e-mail: *duongt@uthscsa.edu*).

Quantitative measurement of Po_2 in vivo could provide a clinically relevant indicator of oxygen concentration in the vitreous and the surrounding tissue, such as the retina, lens, and ciliary body. Abnormal vitreal oxygen tension has been linked to a number of ocular diseases, including cataract, diabetic retinopathy, and central retinal vein occlusion (1–4). Vitrectomy (1,5) and hyperbaric oxygen therapy (6) have been associated with increased incidence of nuclear cataract, likely related to high vitreal Po_2 and reactive oxygen species contributing to cataract formation (7).

Most intraocular Po_2 measurements have been made in humans and animals by using invasive polarographic oxygen electrodes or fiberoptic probes (1,8). Their invasive nature limits human studies to during clinically necessary surgical procedures, such as vitrectomy. As a result, measurement of vitreous Po_2 from healthy humans has not been obtained, and only comparisons of vitreal Po_2 between subjects with different diseases or stages of disease have been made.

Magnetic resonance (MR) imaging offers an alternative method to image vitreal Po_2 noninvasively. The longitudinal relaxation rate, or R1, of water protons is linearly correlated with dissolved oxygen concentration (9) because the dissolved oxygen is a paramagnetic agent. In low-protein body fluids, such as cerebrospinal fluid and the vitreous humor, dissolved oxygen is a dominant source of R1 relaxation. Thus, Po_2 in vivo can be noninvasively determined by measuring R1 of fluids if the relationship between water R1 and oxygen is known. MR imaging application to noninvasively measure Po_2 of body fluids, including cerebrospinal fluid, the vitreous, and urine, in humans has been reported (9). Vitreous Po_2 values reported from MR imaging and by using invasive techniques differed and need further investigation (9). Moreover, vitreal R1 measurements are potentially affected by proteins and ions, the gel-like structure of the vitreous, the temperature gradient across the eye, and the influence of ambient air. These factors have not yet been systematically investigated. The purpose of this study was to characterize these factors and to develop an MR imaging approach to noninvasively image quantitative Po_2 in the human vitreous.

Advances in Knowledge

- MR imaging offers a noninvasive method to image Po_2 in the vitreous by measuring the R1 of water protons, but factors other than oxygen that modulate vitreal R1, such as vitreal macromolecules, gel-like property, and temperature, should be taken into account.
- Calibrations with ex vivo eye and graded Po_2 and temperature phantoms account for the effects of proteins and ions and the gel-like matrix of the vitreous on R1.
- Comparison between eye-open and eye-closed conditions shows spatially dependent R1 differences corresponding to temperature differences of 0.34°–0.83°C, consistent with temperature gradients across the eye.
- In vivo human vitreous Po_2 maps are spatially heterogeneous, with an average whole vitreous Po_2 of 16.7 mm Hg ± 6.5 measured by using MR imaging.

Materials and Methods

Phantom and ex Vivo Studies

Phantoms were made by using distilled water bubbled with nitrogen to Po_2 ranging between 12 and 95 mm Hg and sealed in filled glass vials with rubber stoppers (n = 10). Oxygen tension (in millimeters of mercury) in phantoms was measured by using an oxygen-sensitive fiberoptic probe (OxyLab; Oxford Optronix, Oxford, England) before and after MR imaging. The average difference between the before and after Po_2 measurements was 1.0 mm Hg ± 5.5 (standard deviation), and the average absolute difference was 3.8 mm Hg. The two measured values that were not significantly different (P = .56, paired t test) were averaged. Ex vivo eyes from a New Zealand albino rabbit (male, 6 months old, weight of 2.12 kg) (Harlan Laboratories, Indianapolis, Ind) and a baboon (female, 18 years old, weight of 23 kg) (Southwest National Primate Research Center, San Antonio, Tex) were enucleated at the time of euthanasia and kept in sealed vials of saline. All measurements were performed within 12 hours after euthanasia. Various properties of the vitreous, including viscosity, have been reported to be relatively stable 72 hours after removal compared with freshly removed vitreous (10). After MR imaging, the fiberoptic probe was inserted into the vitreous through a needle to measure vitreous Po_2. For MR imaging measurements, the sealed phantoms and ex vivo eyes were placed in a custom-made chamber with circulating warm water to equilibrate at variable temperatures (34°, 37°, and 40°C). Animal care committee approval was obtained.

MR imaging studies were performed with a 3.0-T whole-body imager with

Implication for Patient Care

- This approach provides vitreous Po_2, which could potentially be used as an imaging biomarker for ocular diseases such as diabetic retinopathy and cataract.

Published online before print
10.1148/radiol.12120777 **Content code:** HN

Radiology 2013; 266:905–911

Author contributions:
Guarantors of integrity of entire study, E.R.M., T.Q.D.; study concepts/study design or data acquisition or data analysis/interpretation, all authors; manuscript drafting or manuscript revision for important intellectual content, all authors; manuscript final version approval, all authors; literature research, E.R.M., Q.P., T.Q.D.; clinical studies, O.S.E.N.; experimental studies, E.R.M., Y.Z., O.S.E.N., T.Q.D.; statistical analysis, E.R.M., T.Q.D.; and manuscript editing, E.R.M., Q.P., T.Q.D.

Funding:
This research was supported by the National Institutes of Health (grants R01 EY014211, EY018855, and T32 HL007446).

Conflicts of interest are listed at the end of this article.

80 mT/m gradient amplitude (Achieva; Philips Healthcare, Best, the Netherlands). The body radiofrequency coil of the imager was used for signal excitation, and an eight-channel head coil was used for signal reception. R1 measurements were made by using a Look-Locker sequence (11) with a spoiled gradient-echo readout, in which data at 26 inversion times were acquired after a single inversion pulse with minimum inversion time of 103 msec; the equal spacing between inversion times was 264 msec. Images were acquired in two shots with the following parameters: repetition time msec/echo time msec, 6.6/3.2; field of view, 100 × 100 mm; matrix, 100 × 100; partial Fourier factor, 0.8; a single 6-mm section; flip angle, 4°; six to nine repetitions; and 20 seconds between repetitions of the inversion pulse.

Human Studies

Human studies were approved by the institutional review board with informed consent obtained from all subjects and were Health Insurance Portability and Accountability Act compliant. Multiple studies were performed in three healthy volunteers (two men, one woman; age range, 26–28 years), with data obtained in seven total study sessions on different days (two sessions from two subjects and three sessions from one subject). Subject body temperature measured on separate days from the MR imaging study, at a similar time of day, was 36.8°C ± 0.2 (n = 3). A custom-made receive-only oblique eye coil (6 × 7-cm diameter) was used. The body radiofrequency coil of the imager was used for signal excitation. Subjects were imaged in the supine position in a custom-made padded head holder to minimize head motion. R1 was measured similar to the phantom study, with the following exceptions: 6.65/3.2; matrix, 168 × 167; partial Fourier factor, 0.6; a single 5-mm axial section; 21 inversion times with a minimum inversion time of 65 msec; spacing between inversion times of 330 msec; and five repetitions. During each session, MR imaging was performed under two conditions: with eyes open and with the imaged eye closed and covered with gauze. The eye was closed and covered to remove temperature gradient across the eye.

Subjects were asked to fixate on a target without blinking during the data readout (7 seconds). In a previous study, a blinking period of 4–8 seconds was found to be comfortable for healthy subjects (12). For the first acquisition, the subject was asked to keep the eye open and blink as needed between MR imaging data readout (which generated a distinct sound cue) but to otherwise keep his or her eyes open. After the first acquisition, the subject was asked to close the eye being imaged, cover it with gauze, and to fixate with the other eye. With the eye closed, acquisitions were then repeated two to three times over the course of 10–43 minutes.

Data Analysis

Image analysis was performed (E.R.M., 6 years of experience) by using codes written in Matlab (MathWorks, Natick, Mass). Images acquired within a session were aligned by using software (Statistical Parametric Mapping 5, SPM5; Wellcome Trust Centre for Neuroimaging, London, England). Images (approximately 10%) with evident ghosting artifacts were excluded from further analysis. R1 was calculated by using a nonlinear least-squares fit of the data to the Look-Locker equation (11). 1/R1, the equilibrium magnetization (M_0), and the excitation flip angle were fit. Linear regression was used to determine the slope and intercept of R1 as a function of Po_2 at each temperature separately, and the slopes were averaged to give a mean relaxivity, assuming they did not vary significantly over ±3°C. The dependence of 1/R1 on temperature is approximately linear across small temperature ranges (13). Linear regression was used to find the slope and intercept of 1/R1 as a function of temperature for each phantom separately, and their slopes were averaged.

Data were expressed as means ± standard deviations, unless noted otherwise. Comparisons were made by using paired t tests, with P less than .05 indicating a significant difference. To evaluate repeatability and reproducibility, two-way analysis of variance was performed on whole vitreous Po_2 values to partition the variance due to different factors. The last two acquisitions of each session with the eye closed were used as same-session repeats, with subject and session as factors of the two-way analysis of variance. The mean squares between sessions and between subjects were calculated in the analysis of variance, and the remaining mean square variation was attributed as coming from the two same-session repetitions.

Results

Figure 1 shows an anatomic image and the R1 map of six distilled water phantoms and an ex vivo rabbit eye. The R1 differences among phantoms with different oxygen concentrations were visually discernible. At 37°C, R1 of the phantoms ranged from 0.207 to 0.215 sec^{-1}, and Po_2 ranged from 12.3 to 94.5 mm Hg (numbers rounded in Fig 1). R1 of the phantoms increased linearly with Po_2 (Fig 2a). Linear regression of the phantom data yielded a slope ($\Delta R1/\Delta Po_2$) of 2.04×10^{-4} sec^{-1}/mm Hg ± 0.06 (standard error), 2.05×10^{-4} sec^{-1}/mm Hg ± 0.09 (standard error), and 2.11×10^{-4} sec^{-1}/mm Hg ± 0.23 (standard error) at 34°, 37°, and 40°C, respectively, giving an average of 2.07×10^{-4} sec^{-1}/mm Hg ± 0.04. At 37°C, the R1 of deoxygenated water (intercept) was 0.205 sec^{-1}.

The ex vivo vitreous Po_2 values of baboon and rabbit eyes were about 0.3 mm Hg from the fiberoptic probe. Vitreous of the ex vivo eyes had slightly larger R1 (0.209 sec^{-1} ± 0.001 at 37°C) than distilled water, likely because of macromolecules, ions, and gel-like media in the vitreous. Vitreous R1 was essentially identical between the baboon and the rabbit, so these data points are on top of each other in Figure 2a, suggesting that the vitreous properties affect R1 similarly between the two species. If oxygen was assumed to have the same relaxivity in the vitreous as water, the R1 of deoxygenated vitreous was 0.209 sec^{-1} at 37°C. In vivo vitreous Po_2 was

thus calculated by using R1 equals 0.209 sec^{-1} + Po_2 · 2.07 × 10^{-4} sec^{-1}/mm Hg at 37°C. Without this correction, Po_2 values would be overestimated by 22.2 mm Hg ($P < .001$).

R1 of the phantoms decreased with increasing temperature (Fig 2b). Linear regression of 1/R1 versus temperature in the phantoms yielded an average slope (Δ[1/R1]/ΔTemp) of 0.106 sec/°C ± 0.009 ($n = 10$), and the mean of the standard error of the slopes was 0.003. This translated to approximately 23 mm Hg per 1°C difference at physiologic conditions (approximately 37°C and 30 mm Hg).

R1 was essentially linearly related to temperature across the small range of temperatures studied. Therefore, a linear regression of R1 as a function of both Po_2 and temperature was performed on the phantom data. The offset of R1 between phantoms and vitreous was calculated at all three temperatures and averaged, giving a difference of 4.98 × 10^{-3} sec^{-1} ± 1.30. After adding in the offset of the vitreous, the relationship was R1 equals 0.387 sec^{-1} + Po_2 · 2.07 × 10^{-4} sec^{-1}/mm Hg − T · 4.78 × 10^{-3} sec^{-1}/°C, where T is the temperature in degrees Celsius. The standard errors of the slopes of the Po_2 and T coefficients were 0.08 × 10^{-4} sec^{-1}/mm Hg and 0.08 × 10^{-3} sec^{-1}/°C, respectively. Note that if 37°C were entered into this equation, the resulting intercept would be 0.210 sec^{-1}, which is essentially identical to the intercept given previously that was calculated by using only the data at 37°C.

A representative R1 map in a human subject with the eye closed is shown in Figure 3. Maintaining eye fixation on a target during MR imaging signal acquisition with cued blinks minimized eye movement and blink artifacts, which was consistent with previous findings (12). Moreover, the Look-Locker sequence rapidly acquires images for all inversion times, which minimizes artifacts from eye movement compared with conventional R1 imaging sequences that acquire one image at each inversion time.

Figure 4 shows the temporal dynamics of R1 changes with the eye

Figure 1

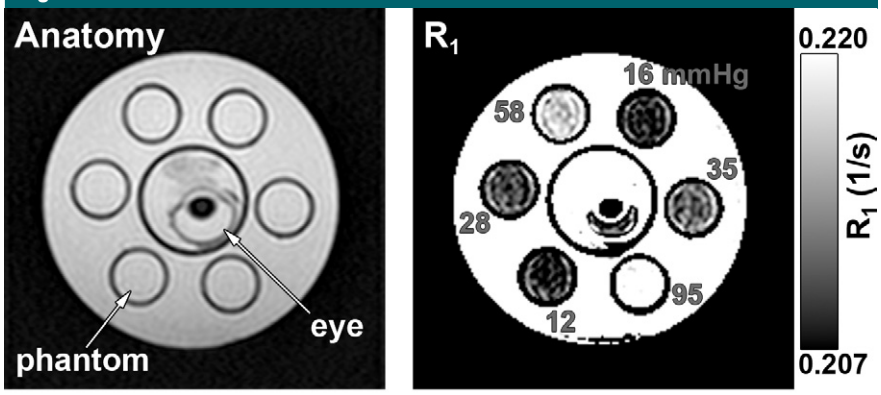

Figure 1: **(a)** Anatomic image (6.6/3.2; inversion time, 636 msec; flip angle, 4°) and **(b)** R1 map (in sec^{-1}) of six phantoms and an ex vivo rabbit eye. The samples are in a chamber filled with warmed water. The numbers on the R1 map are the measured Po_2 (in millimeters of mercury) for each phantom from the fiberoptic probe.

Figure 2

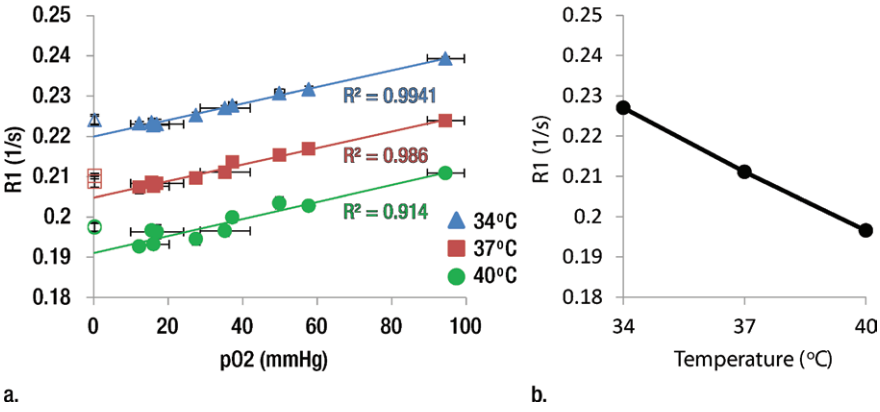

Figure 2: **(a)** Graph shows R1 versus Po_2 of distilled water phantoms (▲, ■, ●) and ex vivo vitreous samples from a rabbit and baboon (△, □, ○) at three temperatures. Vertical error bars are standard deviation of R1 across six to nine repetitions. Horizontal error bars are standard deviation of two fiberoptic Po_2 measurements made before and after MR imaging. **(b)** Graph shows R1 versus temperature from a single phantom (Po_2 = 35.3 mm Hg).

open and closed in a region-of-interest analysis. R1 with the eye closed differed from R1 with the eye open in most regions 10 minutes after closing but did not change further with time. These findings suggest that temperature, not ambient air, is the cause of the difference in R1 between eye open and eye closed.

The group-averaged R1 maps with the eye open and closed and the difference between the two conditions are shown in Figure 5. The whole vitreous R1 differences between the eye open and closed were visually discernible, with the largest differences closer to the anterior part of the eye. Whole vitreous R1 values with the eye open and closed were 0.216 sec^{-1} ± 0.002 and 0.213 sec^{-1} ± 0.001, respectively (P = .004). Assuming this was an effect of temperature, the increases in vitreous temperature in the closed eye (average of all time points) compared with the open eye were as follows: midvitreous, 0.55°C; lens, 0.83°C; anterior temporal

Figure 3

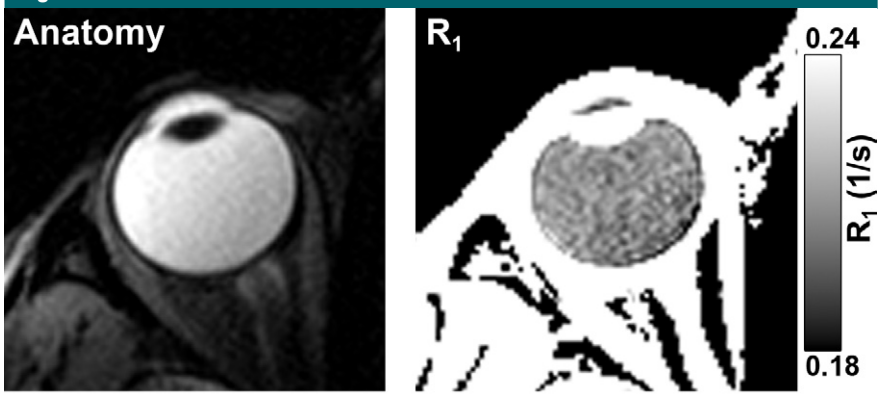

Figure 3: Axial MR images in an in vivo human eye (closed) show **(a)** anatomy (6.6/3.2/395; flip angle, 4°) and **(b)** R1 (in sec^{-1}).

Figure 4

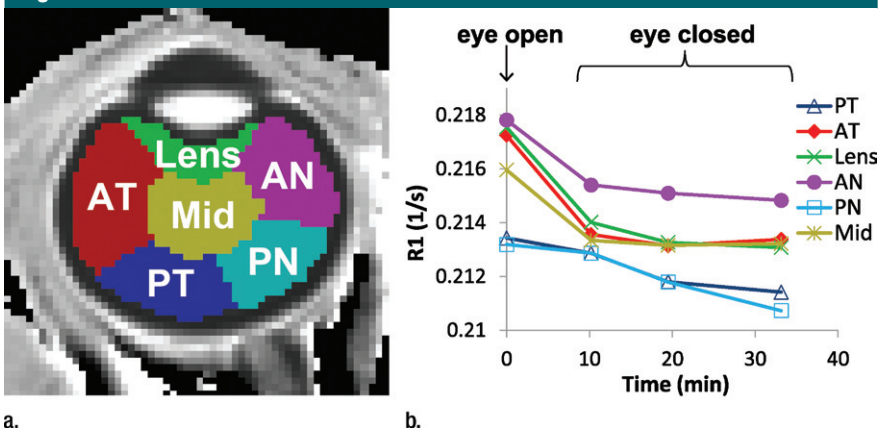

Figure 4: Region-of-interest analysis of changes in R1 between the open and closed eye. **(a)** Axial MR image shows regions of interest. **(b)** Graph shows changes of R1 over time after closing and covering the eye. Data at time of 0 are eye open. Studies acquired at the following times were binned: 9–12 minutes, 15–23 minutes, and 30–43 minutes. *AN* = anterior nasal region, *AT* = anterior temporal region, *Mid* = midvitreous, *PN* = posterior nasal region, *PT* = posterior temporal region.

Figure 5

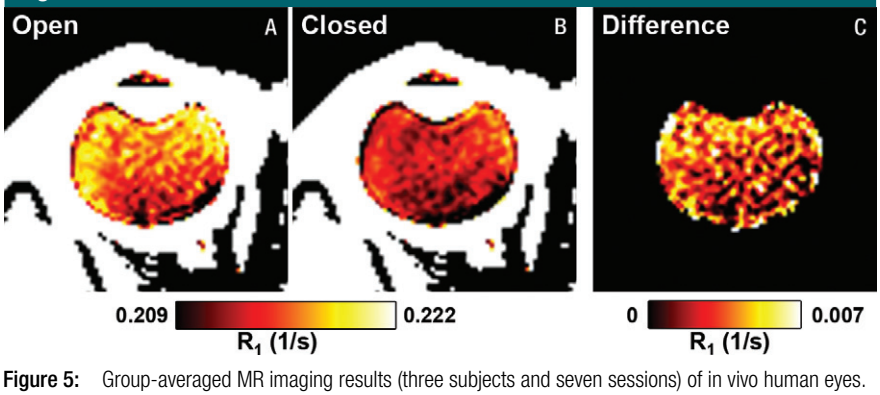

Figure 5: Group-averaged MR imaging results (three subjects and seven sessions) of in vivo human eyes. R1 maps with the eye, *A,* opened and, *B,* closed. *C,* The difference in R1 between open and closed.

region, 0.74°C; anterior nasal region, 0.54°C; posterior temporal region, 0.34°C; and posterior nasal region, 0.36°C (regions of interest shown in Fig 4). These differences in R1 between the open and closed eye would have resulted in error in vitreal Po_2 of 7.9 mm Hg ± 8.5 to 19.8 mm Hg ± 12.5.

Figure 6 shows the group-averaged Po_2 map and Po_2 values of different regions of interest with the eye closed to remove temperature gradients. The Po_2 maps are spatially heterogeneous across the vitreous, with a whole vitreous Po_2 of 16.7 mm Hg ± 6.5. Region-of-interest analysis shows that Po_2 was high in the anterior region and low in the posterior region of the eye. Reproducibility measurements (closed eye) yielded root-mean-square values of 3.3, 10.3, and 10.0 mm Hg for between same-session repetitions, between sessions, and between subjects, respectively.

Discussion

This current study established an MR imaging protocol to image quantitative vitreous Po_2 noninvasively that compared favorably with invasive techniques. Potential effects on R1 measurements from impurities, temperature gradient, and ambient air were evaluated. The vitreous had slightly larger R1 than distilled water, likely because of macromolecules, ions, and gel-like matrix in the vitreous. MR imaging offers spatial resolution that compares favorably to Po_2 electrodes and fiberoptic probes, providing human vitreous Po_2 maps that were spatially heterogeneous. Comparison between eye-open and eye-closed conditions showed spatially dependent R1 differences consistent with ocular temperature gradients. Without corrections for vitreal properties and temperature, human vitreal Po_2 was significantly overestimated.

Invasive oxygen electrodes or fiberoptic probes reported vitreous Po_2 of 7–34 mm Hg (1,3,4,14) in patients during ocular surgery and 13–36 mm Hg in anesthetized healthy rats, rabbits, and cats (14–17) compared with midvitreous Po_2 of 18.3 mm Hg measured with MR imaging in this study.

Figure 6

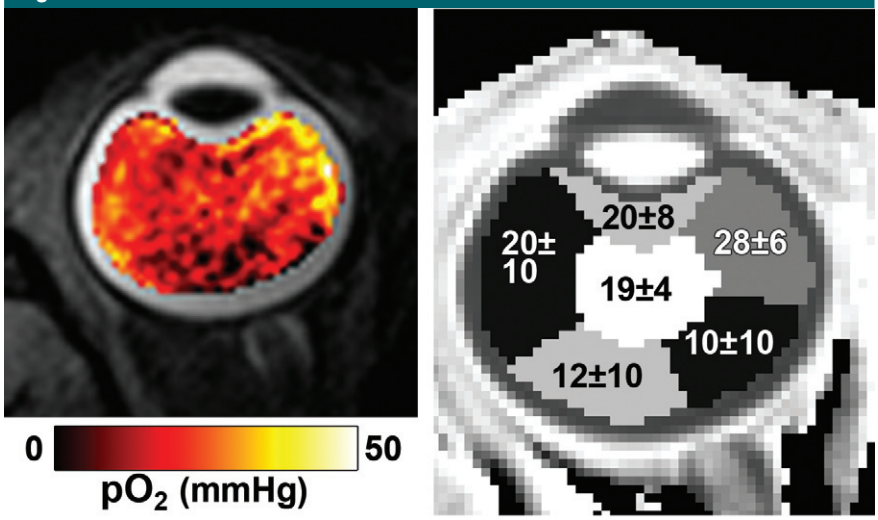

Figure 6: Group-averaged **(a)** Po_2 of the vitreous (eye closed) overlaid on an anatomic image and **(b)** Po_2 values (means ± standard deviations, in millimeters of mercury) with the eye closed for the regions of interest shown.

With MR imaging, Po_2 was higher in the anterior regions and lower in the posterior regions, with midvitreous Po_2 in between. The Po_2 value in the anterior nasal region was higher than the other anterior regions, which were otherwise similar. We are unaware of any studies in humans comparing temporal and nasal vitreous Po_2 or of any reasons that Po_2 should be higher in this one region. Retinal and ciliary body vessels provide oxygen to the vitreous, while the lens consumes oxygen from the vitreous (1). With invasive probes, an oxygen gradient across the vitreous, with Po_2 highest near the retina and lowest in the anterior vitreous, is reported in healthy rabbits (14,17). Spatial dependence of vitreous Po_2 has not been reported in healthy humans. In patients undergoing ocular surgery, midvitreous Po_2 was lower than near the retina (14) and the anterior vitreous (1,14). However, there are reports of lower vitreal Po_2 near the retina than other regions (4,18). These reported regional differences in the human eye are generally small (<4 mm Hg) (1,3,14,18), and different diseases might have different effects on the spatial distribution of Po_2 (3,18).

A previous study using R1 MR imaging at 1.5 T measured whole vitreous Po_2 in healthy subjects to be 63 mm Hg ± 34 (9), which is substantially higher than that of invasive probes and our value. That study found R1 equals 0.213 sec^{-1} + Po_2 · 2.49 × 10^{-4} sec^{-1}/mm Hg in water phantoms at 37°C (9). The relaxivity and intercept were larger than those in our findings, perhaps because of different R1-measurement sequences. Vitreous R1 could be influenced by factors other than oxygen, which affects Po_2 accuracy. Protein (bovine serum albumin) overestimates Po_2 by 11 mm Hg/(grams per liter of protein), but the previous MR imaging–based vitreous Po_2 did not account for this (9). The human vitreous protein content of 0.3–1.4 g/L (19) translates to Po_2 overestimation of 3–15 mm Hg. Ions and the gel structure of the vitreous could also affect R1 but are difficult to account for in phantoms. Without the ex vivo vitreous correction, our whole vitreous Po_2 was 53.5 mm Hg (open eye), similar to the previously reported MR imaging value (9). R1 is also sensitive to temperature, with a relation of 23 mm Hg/°C under physiologic conditions, which is consistent with a previous finding of 19 mm Hg/°C at 1.5 T (9). Normal body temperature could vary by a few degrees (20) and should thus be recorded for accurate Po_2 calculations. The vitreous has temperature gradients of 0.5°–1°C reported invasively in animals (21,22) and from mathematical models of the human eye (23). This is consistent with R1 differences between open and closed eyes which translated to 0.34°–0.83°C, with largest changes anteriorly and smallest posteriorly. The effect of eye closure on vitreous temperature is unknown, but ocular surface temperature can be raised by 1.5°C to more than 3°C by closing the eye (24) or wearing contact lenses (25).

One limitation with MR imaging Po_2 measurement was that oxygen has a relatively small effect on R1, so differences due to sequences or artifacts could significantly affect MR imaging Po_2 values. As such, calibration should be performed for a given pulse sequence and sequence parameters. Another potential limitation was that animal vitreous was used in the calibration. While there are some differences in various vitreous protein concentrations between species (26), rabbit and baboon ex vivo vitreous R1 values were similar. Thus, we expect that the current calibration is applicable to human vitreous as well. Another limitation was that the R1 difference between the open and closed eye has not been confirmed to be entirely due to temperature. An alternative factor contributing to the R1 difference could be oxygen diffusion from ambient air, which occurs in the anterior chamber (27), but is unlikely in the vitreous. Ambient oxygen diffusion is against the primary flow of aqueous humor from the posterior chamber to the anterior chamber (28). Moreover, oxygen diffusion through the vitreous of large eyes is slow, taking more than 10 minutes of oxygen inhalation for vitreous Po_2 to start increasing in the cat eye (16), while R1 changes occurred in less than 10 minutes after closing the human eye. Measurements of proton frequency or apparent diffusion coefficient, which are temperature dependent (29), could be used to independently corroborate temperature differences between the open and closed eye.

Future studies will investigate Po_2 in eye diseases and improve spatial resolution to map Po_2 of the anterior chamber and the vitreous close to ocular tissue interface (such as retina, lens, and ciliary bodies). This approach can be used to establish normative vitreous Po_2 databases for different age, sex, and ethnicity or possibly to measure ocular temperature gradient. Noninvasive MR imaging can provide vitreal Po_2 maps in humans after proper accounting of factors other than oxygen (such as macromolecules, ions, gel structure, and temperature) that could affect vitreal R1.

Disclosures of Conflicts of Interest: E.R.M. No relevant conflicts of interest to disclose. **Y.Z.** Financial activities related to the present article: author receives graduate stipend (Translational Science Training across Disciplines program at the University of Texas Health Science Center at San Antonio). Financial activities not related to the present article: none to disclose. Other relationships: none to disclose. **O.S.E.N.** No relevant conflicts of interest to disclose. **Q.P.** No relevant conflicts of interest to disclose. **T.Q.D.** No relevant conflicts of interest to disclose.

References

1. Holekamp NM, Shui YB, Beebe DC. Vitrectomy surgery increases oxygen exposure to the lens: a possible mechanism for nuclear cataract formation. Am J Ophthalmol 2005;139(2):302–310.
2. Berkowitz BA, Kowluru RA, Frank RN, Kern TS, Hohman TC, Prakash M. Subnormal retinal oxygenation response precedes diabetic-like retinopathy. Invest Ophthalmol Vis Sci 1999;40(9):2100–2105.
3. Maeda N, Tano Y. Intraocular oxygen tension in eyes with proliferative diabetic retinopathy with and without vitreous. Graefes Arch Clin Exp Ophthalmol 1996;234(Suppl 1):S66–S69.
4. Williamson TH, Grewal J, Gupta B, Mokete B, Lim M, Fry CH. Measurement of PO2 during vitrectomy for central retinal vein occlusion, a pilot study. Graefes Arch Clin Exp Ophthalmol 2009;247(8):1019–1023.
5. Thompson JT. The role of patient age and intraocular gas use in cataract progression after vitrectomy for macular holes and epiretinal membranes. Am J Ophthalmol 2004;137(2):250–257.
6. Palmquist BM, Philipson B, Barr PO. Nuclear cataract and myopia during hyperbaric oxygen therapy. Br J Ophthalmol 1984;68(2):113–117.
7. Truscott RJ. Age-related nuclear cataract-oxidation is the key. Exp Eye Res 2005;80(5):709–725.
8. Park YH, Shui YB, Beebe DC. Comparison of two probe designs for determining intraocular oxygen distribution. Br J Ophthalmol 2011;95(1):118–122.
9. Zaharchuk G, Busse RF, Rosenthal G, Manley GT, Glenn OA, Dillon WP. Noninvasive oxygen partial pressure measurement of human body fluids in vivo using magnetic resonance imaging. Acad Radiol 2006;13(8):1016–1024.
10. Aguayo J, Glaser B, Mildvan A, Cheng HM, Gonzalez RG, Brady T. Study of vitreous liquifaction by NMR spectroscopy and imaging. Invest Ophthalmol Vis Sci 1985;26(5):692–697.
11. Brix G, Schad LR, Deimling M, Lorenz WJ. Fast and precise T1 imaging using a TOMROP sequence. Magn Reson Imaging 1990;8(4):351–356.
12. Zhang Y, Nateras OS, Peng Q, et al. Lamina-specific anatomic magnetic resonance imaging of the human retina. Invest Ophthalmol Vis Sci 2011;52(10):7232–7237.
13. Nelson TR, Tung SM. Temperature dependence of proton relaxation times in vitro. Magn Reson Imaging 1987;5(3):189–199.
14. Sakaue H, Negi A, Honda Y. Comparative study of vitreous oxygen tension in human and rabbit eyes. Invest Ophthalmol Vis Sci 1989;30(9):1933–1937.
15. Quiram PA, Leverenz VR, Baker RM, Dang L, Giblin FJ, Trese MT. Microplasmin-induced posterior vitreous detachment affects vitreous oxygen levels. Retina 2007;27(8):1090–1096.
16. Alder VA, Cringle SJ. Vitreal and retinal oxygenation. Graefes Arch Clin Exp Ophthalmol 1990;228(2):151–157.
17. Shui YB, Fu JJ, Garcia C, et al. Oxygen distribution in the rabbit eye and oxygen consumption by the lens. Invest Ophthalmol Vis Sci 2006;47(4):1571–1580.
18. Lange CA, Stavrakas P, Luhmann UF, et al. Intraocular oxygen distribution in advanced proliferative diabetic retinopathy. Am J Ophthalmol 2011;152(3):406–412.e3.
19. Swann DA. Chemistry and biology of the vitreous body. Int Rev Exp Pathol 1980;22:1–64.
20. Sund-Levander M, Forsberg C, Wahren LK. Normal oral, rectal, tympanic and axillary body temperature in adult men and women: a systematic literature review. Scand J Caring Sci 2002;16(2):122–128.
21. Rosenbluth RF, Fatt I. Temperature measurements in the eye. Exp Eye Res 1977;25(4):325–341.
22. Schwartz B. Environmental temperature and the ocular temperature gradient. Arch Ophthalmol 1965;74:237–243.
23. Kunter FC, Seker SS. 3D web-splines solution to human eye heat distribution using bioheat equation. Eng Anal Bound Elem 2011;35(4):639–646.
24. Mapstone R. Determinants of corneal temperature. Br J Ophthalmol 1968;52(10):729–741.
25. Purslow C, Wolffsohn JS, Santodomingo-Rubido J. The effect of contact lens wear on dynamic ocular surface temperature. Cont Lens Anterior Eye 2005;28(1):29–36.
26. Noulas AV, Theocharis AD, Feretis E, Papageorgakopoulou N, Karamanos NK, Theocharis DA. Pig vitreous gel: macromolecular composition with particular reference to hyaluronan-binding proteoglycans. Biochimie 2002;84(4):295–302.
27. Siegfried CJ, Shui YB, Holekamp NM, Bai F, Beebe DC. Oxygen distribution in the human eye: relevance to the etiology of open-angle glaucoma after vitrectomy. Invest Ophthalmol Vis Sci 2010;51(11):5731–5738.
28. Brubaker RF. Flow of aqueous humor in humans [The Friedenwald Lecture]. Invest Ophthalmol Vis Sci 1991;32(13):3145–3166.
29. Quesson B, de Zwart JA, Moonen CT. Magnetic resonance temperature imaging for guidance of thermotherapy. J Magn Reson Imaging 2000;12(4):525–533.